ELSEVIER

Journal of Photochemistry and Photobiology A: Chemistry 108 (1997) 79–84

Journal of PHOTOCHEMISTRY AND PHOTOBIOLOGY A:CHEMISTRY

Synthesis, characterization and photocatalytic properties of iron-doped TiO_2 catalysts

K.T. Ranjit, B. Viswanathan *

Department of Chemistry, Indian Institute of Technology, Madras 60 036, India

Abstract

Fe-doped TiO_2 catalysts were prepared by coprecipitation and the sol–gel method. The anatase to rutile phase transformation is dependent on the nature of the precursor used. Sol–gel-derived iron-doped catalysts show the presence of rutile and pseudobrookite phases, whereas coprecipitated catalysts show only the anatase phase. The role of the dopant ion is primarily to improve the charge separation of the photoproduced electron–hole pairs via a permanent electric field. The photocatalytic activity of the iron-doped catalysts can be explained in terms of the heterojunction formed between the Fe/TiO_2 and α-Fe_2O_3 phases for the sol–gel-derived catalyst. ©1997 Elsevier Science S.A.

Keywords: Characterization; Iron-doped TiO_2 catalysts; Photocatalytic properties; Synthesis

1. Introduction

Of the many semiconducting oxides, TiO_2 [1–3] is a suitable material. It offers a high light conversion efficiency, mainly due to its stability in aqueous suspensions of different pH value on irradiation and the relatively favourable disposition of its band edges. However, one disadvantage of TiO_2 is that the bandgap energy is approximately 3.2 eV; therefore UV illumination is necessary to photoactivate this semiconductor. Another disadvantage of TiO_2 is that charge carrier recombination occurs within nanoseconds and, in the absence of promoters (e.g. Pt or RuO_2), the photocatalytic activity is low.

Attempts to improve the performance of TiO_2 as a photocatalyst and to extend its light absorption and conversion capacity to the visible portion of the solar spectrum have primarily been concerned with the effect of dopants [4–8]. A wide range of metal ions, in particular transition metal ions, have been used as dopants for TiO_2, and their effects on the properties of the doped samples have been reported [9–11].

Although many studies have been reported on the electrochemical reduction of nitrite and nitrate ions in acidic media, few investigations of the photocatalytic reduction have been performed in neutral medium [12–14]. The purpose of this study is to examine a number of experimental variables which affect the photocatalytic reduction of nitrite and nitrate ions on Fe-doped TiO_2 catalyst.

* Corresponding author. Tel.: +91 44 235 1365; fax: +91 44 235 0509.

PII S1010-6030(97)00005-1

2. Experimental details

2.1. Preparation of doped TiO_2

The doped samples were prepared by coprecipitation and the sol–gel method.

2.1.1. Coprecipitation method

In the coprecipitation method, iron and titanium hydroxide were coprecipitated by reacting an aqueous solution of $TiCl_4$ containing Fe^{3+} ions with vigorous stirring owing to the exothermicity of the reaction. The solid was filtered and washed repeatedly to remove Cl^- (tested as AgCl(s)). After standing for 24 h at room temperature, the solid was dried at 383 K for 24 h and calcined in air at 823 K for 24 h. The temperature of 823 K for calcination was chosen for two reasons, namely crystallization only occurred on heating at 823 K for 24 h and the impregnated and coprecipitated samples showed an endotherm around 723 K due to the decomposition of adsorbed nitrate.

2.1.2. Sol–gel method

Iron-doped TiO_2 was prepared by the acid-catalysed sol–gel method. The sol was prepared by mixing Ti(IV) isopropoxide with anhydrous 2-propanol, water, nitric acid and iron nitrate with stirring. Three different sols were prepared with varying ratios of alcohol and water content and different molar ratios between Ti(IV) isopropoxide and acid. The gel obtained was dried in an air oven at 383 K for 12 h. Crystallization occurred in air by heating at 823 K for 24 h.

2.2. Estimation of metal loading

The dopant concentration in the catalyst was analysed by inductively coupled plasma atomic emission spectrometry (ICPAES; model 3410, ARL) after calibration with a standard metal solution.

2.3. X-Ray diffraction (XRD) studies

X-Ray diffractograms were obtained for powdered samples with a Philips diffractometer (Philips Generator, Netherlands; model PW 1130) provided with an on-line recorder and dot-matrix printer (Tele type, USA). The diffraction patterns were recorded at room temperature using Ni-filtered Cu Kα radiation ($\lambda = 1.5418$ Å) for all the samples. A scanning speed of 3° min^{-1} and a chart speed of 5 mm deg^{-1} were employed.

2.4. Thermogravimetry (TG) and differential scanning calorimetry (DSC) studies

TG and DSC experiments of some of the catalysts were carried out using a Perkin–Elmer TGA-DSC-7 instrument in the temperature range 322–873 K for TG studies and 323–773 K for DSC studies in air. A flow rate of 20 ml min^{-1} and a heating rate of 20 °C min^{-1} were employed for all the samples.

2.5. Surface area (SA) studies

The SAs of the samples were measured by N_2 adsorption at 77 K using the dynamic Brunauer–Emmett–Teller (BET) method with a Carlo Erba (model 1800) sorptometer. The samples were outgassed in an evacuation chamber to a pressure of 10^{-3} atm at 393 K prior to adsorption.

2.6. Diffuse reflectance spectroscopic studies

A Hitachi spectrophotometer (model 150-20) equipped with an integrating sphere was used to record the diffuse reflectance spectra of the samples. The baseline correction was performed using a calibrated sample of barium sulphate. The spectra were recorded at room temperature in air in the range 350–900 nm. The same spectrophotometer was used to record the UV absorption spectra of the solutions.

2.7. Photocatalytic studies

The photocatalytic experiments were performed in an all-glass static system at ambient temperature and atmospheric pressure. In all the experiments, 100 mg of the freshly prepared catalyst and 20 ml of the appropriate solution (sodium nitrite and sodium nitrate of appropriate concentration for nitrite and nitrate reduction) were placed in a double-walled cylindrical Pyrex glass reactor. The reactor was equipped with water circulation in the outer jacket in order to maintain a constant temperature and to act as an IR filter. The reaction mixture was stirred at a constant speed during illumination by a magnetic stirrer. The suspension was irradiated using a 450 W Xe lamp (Oriel Corporation, USA). Argon gas was purged when nitrite (nitrate) solutions were illuminated. Before starting the illumination, the reaction mixture was stirred for 30 min in the dark. After irradiation, the solution was centrifuged to remove essentially all the catalyst and the centrifugate was analysed for ammonia.

2.8. Estimation of ammonia

Ammonia was estimated by the indophenol blue method [15].

2.9. Electron spin resonance (ESR) studies

ESR spectra were recorded at the X band on a Varian (E Line Century Series) spectrometer at ambient conditions of temperature and pressure using DPPH ($g = 2.0036$) as the reference.

3. Results and discussion

3.1. Coprecipitated iron-doped TiO_2 catalysts

The X-ray diffraction patterns of the coprecipitated samples show peaks corresponding to the anatase phase of TiO_2 only. No peaks due to haematite (Fe_2O_3) are observed in any of the samples. Hence it is concluded that the incorporation of iron in these catalysts does not catalyse the anatase to rutile phase transformation, at least at the temperatures at which these catalysts are calcined. The calculated lattice parameters show that, with increasing iron content, there is an increase in the unit cell volume, but beyond a certain value the unit cell volume decreases. The ionic radius of Fe^{3+} is 0.64 Å, whereas that of Ti^{4+} is 0.68 Å. The increase in the unit cell volume indicates that Fe^{3+} does not replace Ti^{4+} in the lattice, but forms a solid solution. The characteristics of iron-doped samples prepared by the coprecipitation method are given in Table 1.

Table 1
Characteristics of iron-doped samples

Specimen	Fe content (wt.%)	Surface area ($m^2 g^{-1}$)	Unit cell volume (Å^3)
CP-1	0.11	52.4	136.58
CP-2	0.13	82.9	136.79
CP-3	0.28	35.9	136.89
SG-1	0.29	12.1	–
SG-2	1.48	N.D.	–
SG-3	1.76	3.2	–

N.D., not determined.

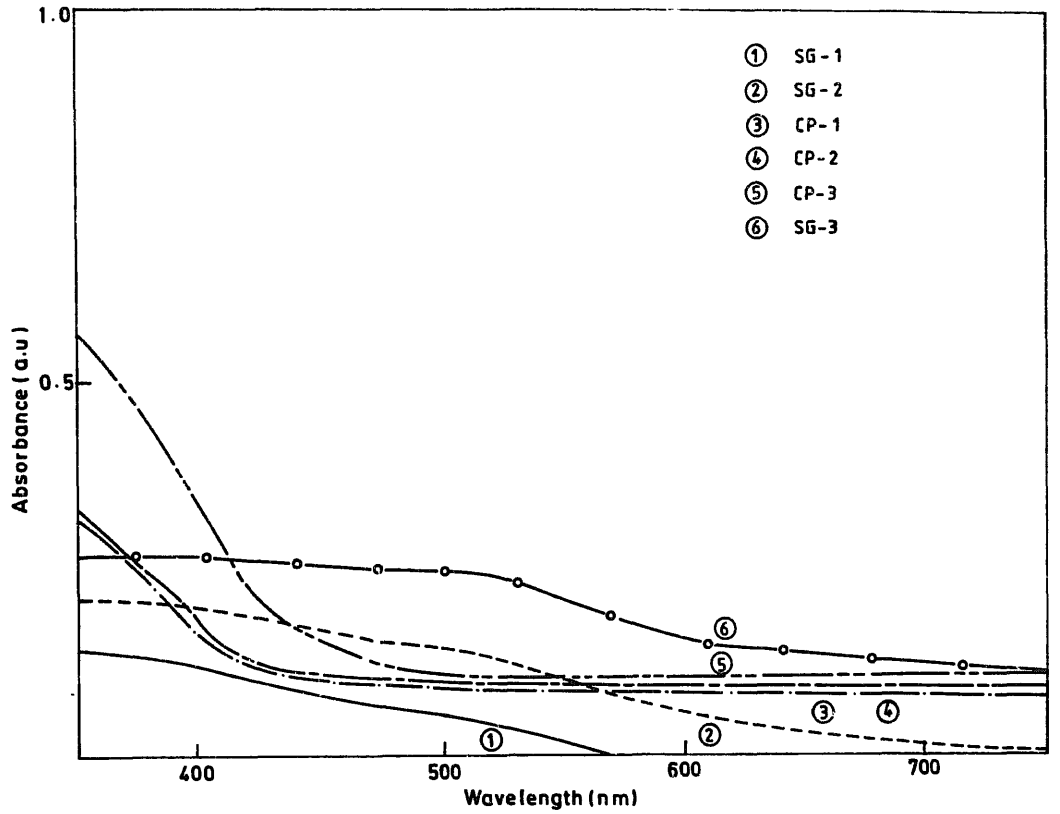

Fig. 1. Diffuse reflectance spectra of iron-doped TiO_2 catalysts.

TG analysis and DSC studies of the coprecipitated samples show a small endothermic peak at approximately 723 K. This is due to the decomposition of adsorbed nitrate, which is used as the precursor. These results corroborate the fact that no rutile phase is present in these catalysts.

The diffuse reflectance spectra of the specimens (Fig. 1) show that the onset of absorption is shifted to longer wavelengths with increasing iron content. In addition, the absorbance of the samples increases with increasing iron content.

The ESR spectrum of the coprecipitated sample containing 0.28 wt.% Fe (see Fig. 2(a)) consists of an intense line at $g = 1.988$ with a symmetric shape. This can be assigned to "isolated" Fe^{3+} ions in the anatase phase [16].

The photocatalytic activity of iron-doped TiO_2 catalysts was examined and the results obtained are given in Table 2. Since this is a comparative study, the amount of ammonia formed after 2 h of irradiation alone was measured (the amount of ammonia formed in this time period is within measurable limits). No kinetic studies were attempted since the amount of ammonia formed is low at short intervals. The error in the estimation of ammonia is ± 0.05 μmol.

When TiO_2 is doped with a p-type donor, the rate of ammonia production is expected to decrease monotonically with increasing dopant concentration [15]. Indeed, this behaviour is observed, i.e. the yield of ammonia (expressed per unit SA of the catalyst) decreases with increasing iron content after passing through a maximum. However, the pure TiO_2 semiconductor does not exhibit any activity. Thus the increase in activity on doping with iron can be attributed to the increase in lifetime of the electron–hole pairs. Another important factor is that the diffusion length of the minority carriers is also influenced by the presence of iron species (2 μm for Fe-doped TiO_2 compared with 1 μm for TiO_2 [4]).

3.2. Sol–gel-derived catalysts

The X-ray diffractograms of the sol–gel-derived catalysts show peaks due to rutile and pseudobrookite phases. No X-ray diffraction peaks due to anatase are observed for any of the sol–gel-derived catalysts.

The reactant composition and time required for gelation are given in Table 3.

The sol–gel process includes two steps. The first step is the hydrolysis of the metal alkoxide and the second step is polymerization. Since the process is acid catalysed, the rate of hydrolysis will increase with increasing acid concentration. However, this has no direct effect on the gelation time.

The characteristics of the iron-doped samples prepared by the sol–gel method are given in Table 1.

It is observed that the catalysts prepared with a large ROH/Ti ratio have a higher SA. Diluting the reactants with the host medium has the effect of separating the molecules and favouring those reactions which depend less on the diffusion of the larger species. Thus hydrolysis reactions are favoured compared with polymerization reactions at high ROH/Ti ratios. Consequently, the particle size decreases with dilution and hence SG-1 exhibits a higher SA (see Table 1).

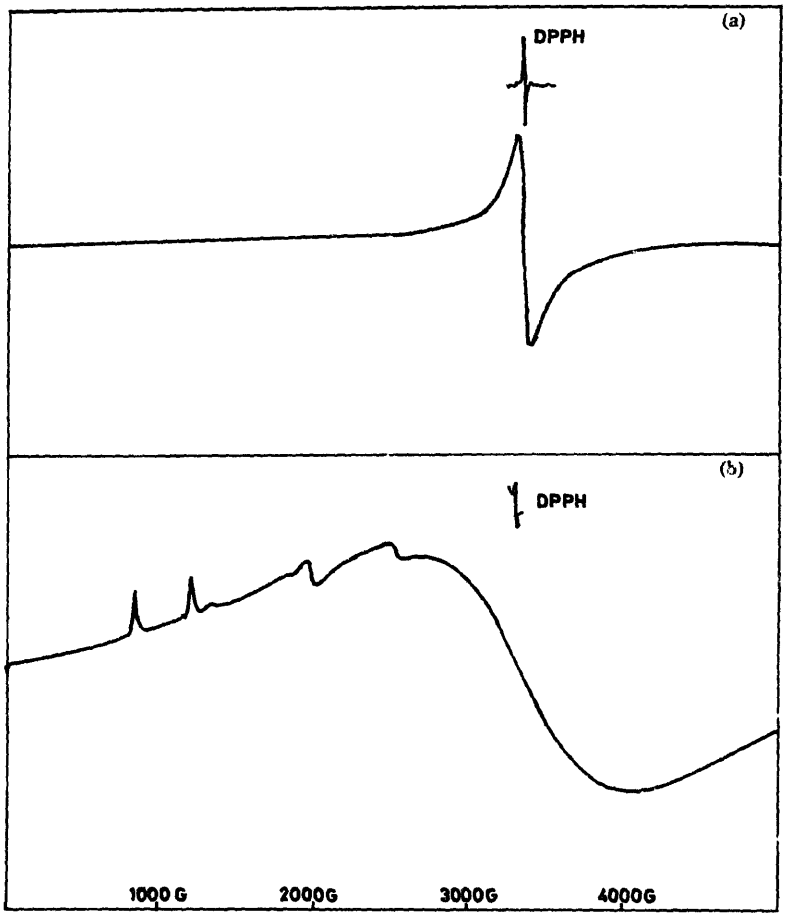

Fig. 2. ESR spectra of iron-doped TiO_2 catalysts.

Table 2
Photocatalytic activity of iron-doped TiO_2 catalysts

Catalyst	Fe content (wt.%)	Yield of ammonia (μmol)	
		$NO_2^- \rightarrow NH_3$	$NO_3^- \rightarrow NH_3$
CP-1	0.11	0.41	0.25
CP-2	0.13	0.78	0.45
CP-3	0.28	0.35	0.07
SG-1	0.29	0.38	0.19
SG-2	1.48	2.84	0.36
SG-3	1.76	0.08	–

Reaction conditions: 20 ml of nitrite (nitrate), 2 h irradiation, 100 mg catalyst.

Table 3
Reactant compositions for sol–gel-derived catalysts

Specimen	Temperature (K)	H_2O/Ti	ROH/Ti	Ti : HNO_3	Gelation time (h)
SG-1	318	18	41	0.44	20
SG-2	308	25	20	1.25	24
SG-3	308	30	23	1.30	2

ROH, 2-propanol.

The diffuse reflectance spectra of the sol–gel-derived iron-doped catalysts are shown in Fig. 1. With an increase in iron content, enhanced absorption is observed in the visible region.

The ESR spectrum of the sol–gel-derived catalyst SG-1 is shown in Fig. 2(b). The peaks can be assigned to Fe^{3+} ions substituting for Ti^{4+} in the TiO_2 rutile lattice [17].

The photocatalytic activities of the sol–gel-derived iron-doped TiO_2 catalysts were examined and the results obtained are given in Table 2. For the sol–gel-derived catalysts, there is an optimum iron content.

The diffuse reflectance spectra of the sol–gel-derived catalysts exhibit high absorbance due to the accumulation of iron-rich layers at the surface. The heterojunction formed by the contact between the two chemically distinct phases plays an important role in determining the activity of the catalysts.

The negligible activity exhibited by the heavily doped catalyst, namely SG-3, can be explained as follows. The factor that can contribute to this low activity is a simple optical screening effect, in which the iron oxide surface phase absorbs all of the electromagnetic radiation and the core phase cannot be activated directly. The existence of Anderson states has been proposed by Bickley et al. [18]. Accordingly, a similar condition can be expected to prevail in the overlayer

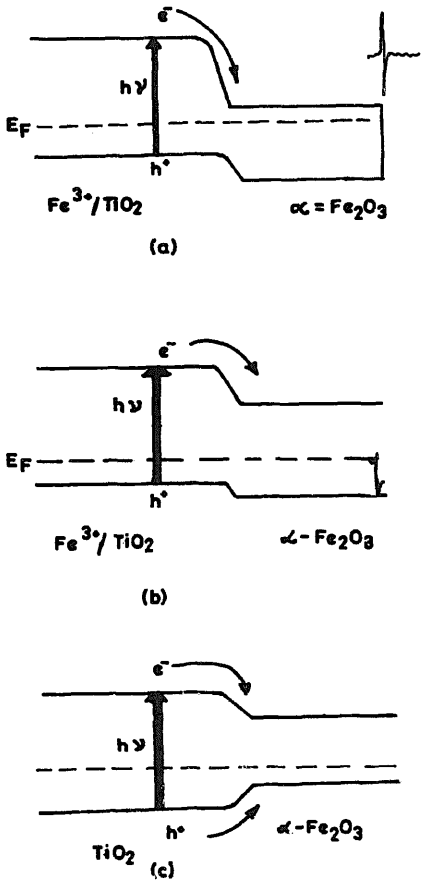

Fig. 3. Heterojunctions formed between Fe_2O_3 and TiO_2 catalysts.

of iron(III) oxide when the anatase to rutile phase transition occurs. This transition is assisted by the presence of anion vacancies, creating Fe^{3+} ions, which result in the precipitation of the iron-rich oxide layer, since the rutile phase has a lower limit of solubility [16] for Fe^{3+} than the anatase phase. Since the observed effect of the overlayer is to cause deactivation, it is assumed that the existence of Anderson states in the overlayer promotes a favourable condition for electron–hole recombination [19] as illustrated in Fig. 3(c).

In catalysts SG-1 and SG-2, the iron-saturated TiO_2 matrix need not necessarily be covered entirely by iron(III) oxide or Fe_2TiO_5. Thus the screening effect may operate over a portion of the external surface, but activation of the remaining portion of the iron-saturated surface is possible. Thus these two specimens exhibit moderate activity. The different kinds of heterojunction formed between TiO_2 and the α-Fe_2O_3 phase are depicted in Fig. 3.

In the specimen SG-1, the contact between the doped TiO_2 matrix and the α-Fe_2O_3 phase is depicted in Fig. 3(b). Electron transfer from the Fe/TiO_2 phase to the iron oxide is facilitated, while hole transfer has an activation energy of 5–10 kJ mol^{-1}. In specimen SG-2, a similar circumstance prevails for the conduction band electrons, but the magnitude of the activation energy for hole transport into the iron oxide is approximately 30–40 kJ mol^{-1}, with electron–hole recombination less favoured as shown in Fig. 3(a).

4. Conclusions

The following conclusions can be drawn from the present investigation.

1. The anatase to rutile phase transformation is dependent on the nature of the precursor used. Sol–gel-derived iron-doped catalysts show the presence of rutile and pseudo-brookite phases, whereas coprecipitated catalysts show only the anatase phase of TiO_2.
2. The onset of absorption is shifted to longer wavelengths on doping TiO_2 with Fe cations. In addition, the absorbance values increase with increasing dopant concentration.
3. The role of the dopant ion is primarily to improve the charge separation of the photoproduced electron–hole pairs via a permanent electric field.
4. An increase in dopant ion content favours electron–hole separation and therefore enhances the photoactivity. However, beyond a certain level, the space charge layer becomes thicker, and the probability of carrier recombination is increased. Thus there is an optimal value at which the photoactivity reaches a maximum.
5. Doping of TiO_2 may influence the adsorption of the reagent species (the equilibrium dark adsorption of nitrite is higher for doped catalysts than for pure TiO_2) and may also induce a displacement of the Fermi level. This displacement does not seem to affect the effectiveness of the electron–hole pair separation with respect to that of pure TiO_2.
6. The resulting photoactivity of the doped catalysts derives from a balance of the above factors, some of which play contrasting roles.

References

[1] E. Pelizzetti, V. Carlin, C. Minero, M. Graetzel, New J. Chem. 15 (1991) 351.
[2] H. Hidaka, J. Zhao, E. Pelizzetti, N. Serpone, J. Phys. Chem. 96 (1992) 2226.
[3] L.A. Dibble, G.B. Raupp, Catal. Lett. 4 (1990) 345.
[4] H.P. Maruska, A.K. Ghosh, Solar Energy Mater. 1 (1979) 237.
[5] E. Borgarello, J. Kiwi, E. Pelizzetti, M. Visca, M. Grätzel, J. Am. Chem. Soc. 103 (1981) 6324.
[6] J. Kiwi, C. Morrison, J. Phys. Chem. 88 (1984) 6146.
[7] W.K. Wong, M.A. Malati, Sol. Energy 2 (1986) 163.
[8] J. Kiwi, M. Grätzel, J. Phys. Chem. 90 (1986) 637.
[9] A. Davidson, M. Che, J. Phys. Chem. 96 (1992) 9909.
[10] Z. Luo, Q.-H. Gao, J. Photochem. Photobiol. A: Chem. 63 (1992) 367.
[11] M.M. Hukovic, M.C. Ceric, Mater. Res. Bull. 23 (1988) 1535.
[12] K.T. Ranjit, R. Krishnamoorthy, B. Viswanathan, J. Photochem. Photobiol. A: Chem. 81 (1994) 55.
[13] K.T. Ranjit, R. Krishnamoorthy, T.K. Varadarajan, B. Viswanathan, J. Photochem. Photobiol. A: Chem. 86 (1995) 185.

[14] K.T. Ranjit, T.K. Varadarajan, B. Viswanathan, J. Photochem. Photobiol. A: Chem. 89 (1995) 67.
[15] K.E. Karakitsou, X.E. Verykios, J. Phys. Chem. 97 (1993) 1184.
[16] D. Cordischi, N. Burriesci, F. D'Alba, M. Petrera, G. Polizzotti, M. Schiavello, J. Solid State Chem. 56 (1985) 182.
[17] N.G. Maksinov, I.L. Mikhailova, V.F. Anufrenko, Kinet. Catal. 13 (1973) 1162.
[18] R.I. Bickley, T.G. Carreno, A.R.G. Elipe, G. Munuera, L. Palmisano, J. Chem. Soc., Faraday Trans. 90 (1994) 2257.
[19] R.I. Bickley, G. Munuera, F.S. Stone, J. Catal. 31 (1973) 398.